

Wit GRZESIK<sup>1</sup>  
Piotr NIESLONY<sup>1\*</sup>  
Witold HABRAT<sup>2</sup>  
Piotr LASKOWSKI<sup>3</sup>

## **INFLUENCE OF CUTTING CONDITIONS ON TEMPERATURE DISTRIBUTION IN FACE MILLING OF INCONEL 718 NICKEL-CHROMIUM ALLOY**

This paper presents 3D FEM simulation results obtained for the milling operations on a nickel-chromium alloy (Inconel 718) using the Johnson-Cook material constitutive model and variable cutting conditions. Face milling tests were carried out using silicon-aluminum-oxygen-nitrogen (SiAlON) ceramic cutting tools inserts. The machining conditions were selected based on real production data (cutting speed of  $v_c=750$  and  $800$  m/min, feed of  $f=0.1$ ,  $0.125$  and  $0.15$  mm/t, depth of cut of  $a_p=1$ ,  $1.5$  and  $2$  mm). The FEM simulations include the maximum and average values of the cutting temperature. They were compared with experimental data obtained by using the high speed infra-red camera.

### **1. CONSTITUTIVE MATERIAL MODELS FOR FEM SIMULATION**

Development of manufacturing processes requires new and robust methods of technological process optimization which are tested in the implementation phase. For instance, in the machining practice engineers modify tool paths by means of the selection of the technological parameters and cutting tool configurations. All of these activities are based on expensive experiments and technological tests in production environment.

At present, the FEM based simulation is a basic engineering tool which accelerates and facilitates the successful solution of this problem. However, the basic obstacle in the engineering application of the FEM technique is the lack of an accurate constitutive material model which will cover a wide spectrum of both the workpiece and cutting tool materials [1],[2],[3]. In particular, more accurate and complete constitutive material models which consider the appropriate mechanical thermophysical properties of both the workpiece and tool materials are needed [4],[5],[6]. A distinct controversy appears in the modelling of aerospace construction materials, including the heat resistant superalloys (HRSA),

---

<sup>1</sup> Opole University of Technology, Dept. of Manufacturing Engineering and Process Automation, Opole, Poland

<sup>2</sup> Rzeszów University of Technology, Dept. of Manufacturing Techniques and Automation, Rzeszów, Poland

<sup>3</sup> WSK PZL Rzeszów, Poland

\* E-mail: p.nieslony@po.opole.pl

basically a group of titanium and nickel-based alloys [2],[7],[8]. The elaboration of an accurate constitutive model depends on the following important technical possibilities and limitations:

- Determination of mechanical properties of the workpiece material under real cutting conditions [9],[10],
- Identification of the thermophysical properties of the workpiece and cutting tool materials taking into account the deposited coatings [11],[12],
- Quantification of friction in the cutting zone [13],[14],
- Considering chip segmentation mechanism in machining [15],[16].

The determination of the appropriate parameters of the constitutive material model requires numerous experimental tests and data analyses. In particular, reverse solutions have also been proposed [17]. Current trends show that the FEM constitutive model should satisfy the High Speed Cutting (HSC) and High Performance Cutting (HPC), which require the implementation of high strain rate tests. Moreover, the material modelling should cover a wide spectrum of cutting tool materials including multilayer coated and composite tools.

Taking into consideration all these facts, the paper is, in general, focused on the influence of the basic constitutive model of the workpiece material, Johnson-Cook (JC), on the results and simulation accuracy when performing 3D flat milling operations using SiAlON rounded inserts to machine an Inconel 718 nickel-chromium alloy. An important aspect of the generation of material constitutive models is to determine accurately their parameters based on the experimental data.

## 2. EXPERIMENTAL METHODOLOGY

The tests were carried out for a flat milling with tree-flute cutter-head type KSSR050RN12CF03 with SiAlON inserts type RNGN120700E KY1540 from KENNAMETAL. The 3D CAD model of the rounded ceramic cutting insert with FEM meshing strategy 1a and the model of the tool edge used in FEM simulation 1b are presented in Fig. 1. To reduce the FEM calculation time the tool insert was created as a rigid non-deformable model with a thickness of 0.2 mm. In order to obtain the increase of the nodal mesh density at the junction between the cutting edge and the workpiece material, the settings of AE were modified. The meshing strategy was realized based on own matching parameter data [18] presented in Fig. 1 such as maximum and minimum tool element size, mesh grading etc. This also results in the increase of the mesh density in the cutting zone (Fig. 1b) and allows achieving a significant increase in the number of nodes in the area of workpiece material after machining.

The defined tool insert model with appropriate settings resulting from its location in the cutter head were imported correctly to the FEM simulation system. The CAD model of the cutter head with three rounded inserts is shown in Fig. 2. The experimental and simulation conditions are specified in Table 1. Additionally, it was necessary, looking at FEM simulation method, to determine the initial angle of head rotation  $\phi_0 = 37^\circ$ . Fig. 3 visualizes technological parameters introduced in FEM package along with the coordinate system  $xyz$  and initial angle of head rotation  $\phi_0$ .

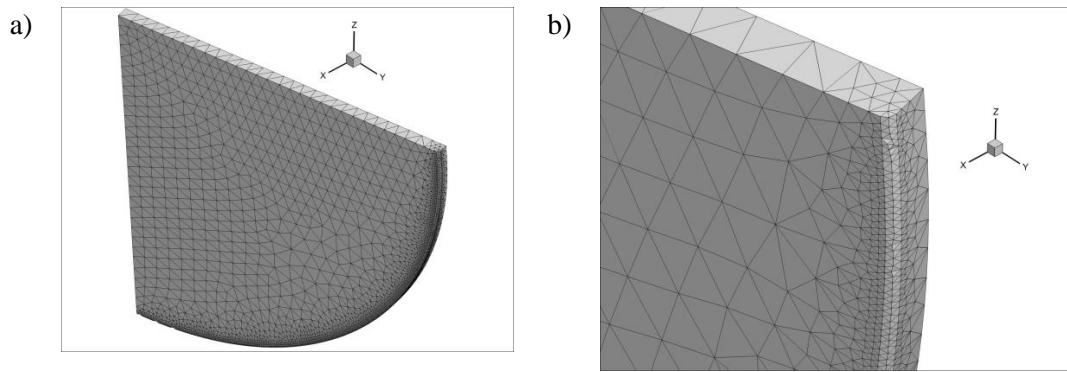


Fig. 1. FEM meshing of the cutting tool model type RNGN120700E KY1540 (a) with cutting edge area for used meshing parameters (b): Maximum (0.3 mm) and minimum (0.03 mm) tool element size, minimum edge length (0 mm), mesh grading (0.5), curvature safety (1.5), segments per edge (0.5)

Table 1. Conditions of numerical and experimental tests

|                          |  |   |
|--------------------------|--|---|
| Workpiece                | Inconel 718  |   |
| Technological parameters | $v_c=750, 800$ m/min,<br>$a_p=1.0, 1.5, 2.0$ mm                                    | $a_e=10$ mm<br>$f_z=0.1, 0.125$ and $0.15$ mm/tooth |
| Cutting tool             | Cutting tool insert: RNGN120700E KY1540<br>Material: ceramic type SiAlON, uncoated |   |
| Constitutive model       | Johnson-Cook (JC) with defined thermo-physical parameters                          |   |
| Friction coefficient     | 0.5 (in FEM simulations)   |   |
| Type of FEM simulation   | Three-dimensional (3D)   |   |

The objective of this study is to compare the experimental results with simulation data obtained for Johnson-Cook model (JC) constitutive material model, which is predominantly used for modelling of machining processes of metallic alloys [2]. The parameters for the JC constitutive model used in this study are specified in Table 2.

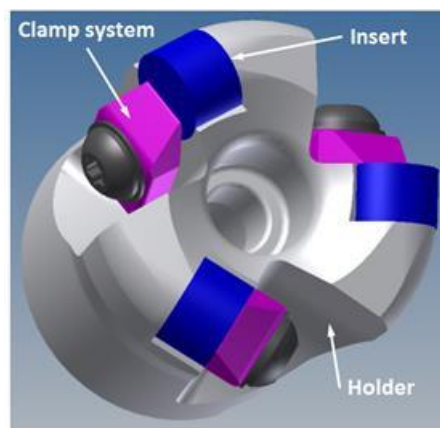


Fig. 2. CAD computer model of a milling cutter head denoted by symbol KSSR050RN12CF03

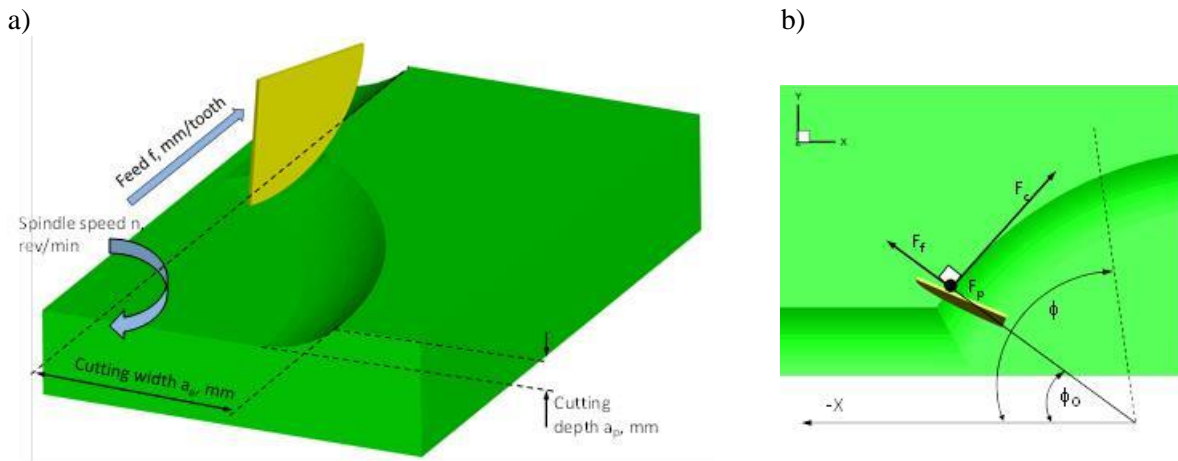


Fig. 3. Technological parameters (a) and axes with defined vectors of cutting force components in the FEM system (b). Fixed initial angle of head rotation  $\phi_0=37^\circ$

Experimental research was carried out on CNC DMU 80P duoBLOCK milling machine equipped with a HD infra-red camera, model X6540sc (Fig. 4a). The emissivity coefficient for the Inconel 718 alloy was determined to be equal to 0.35. During the tests, maximum temperatures in cutting zone were recorded (Fig. 4b) using the flying point algorithm method. The values of the maximum temperature were calculated as an average of obtained maximum values for every contact of cutting edge with workpiece during machining.

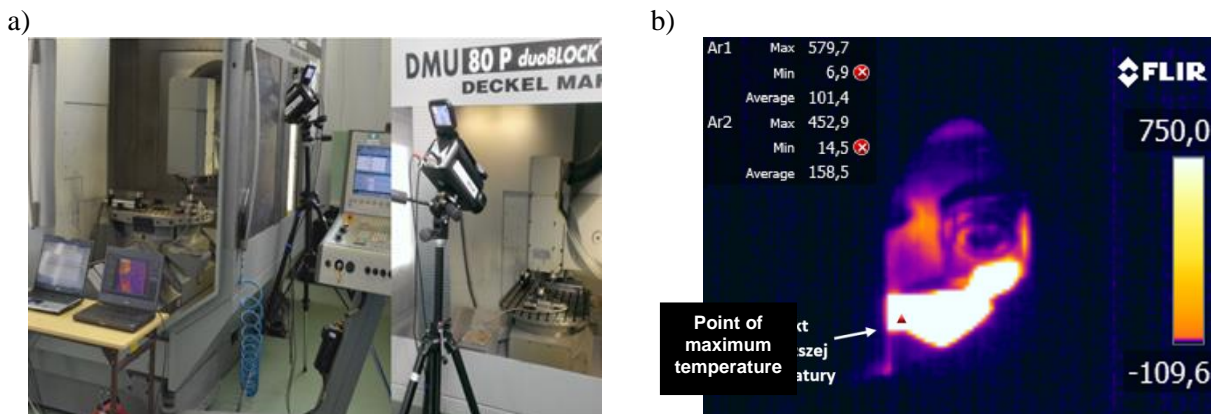


Fig. 4. Temperature measurement in milling process using HD infra-red camera X6540sc (a) and a sample sequence recorded with measuring point of the maximum temperature (b)

In order to consider the thermophysical properties of Inconel 718 alloy, own input data were implemented into the JC model. They concern the measured values of the thermal conductivity (Fig. 5a) and specific heat (Fig. 5b) of the nickel based alloy in the function of temperature. In order to compare them with literature data some plausible values from MPDB data base [19] were entered into the figure.

It can be noted in Figs. 5a and 5b that the differences between literature and experimental data are not distinct, especially for the thermal conductivity (Fig. 5a). Moreover, the trend for the behaviour of the specific heat agrees with literature data.

Table 2. Johnson – Cook (JC) constitutive model parameters [10],[17],[19]

| Parameter                        | A, MPa                  | B, MPa | n    | C     | m   | $\dot{\epsilon}_p^0$ , 1/s |
|----------------------------------|-------------------------|--------|------|-------|-----|----------------------------|
|                                  | 450                     | 1700   | 0.65 | 0.017 | 1.3 | 1.0                        |
| Melting temperature              | 1260°C                  |        |      |       |     |                            |
| Young module                     | 200 GPa                 |        |      |       |     |                            |
| Poisson's ratio                  | 0.294                   |        |      |       |     |                            |
| Coefficient of thermal expansion | $1.2 \cdot 10^{-5}$ 1/K |        |      |       |     |                            |
| Density                          | 8206 kg/m <sup>3</sup>  |        |      |       |     |                            |

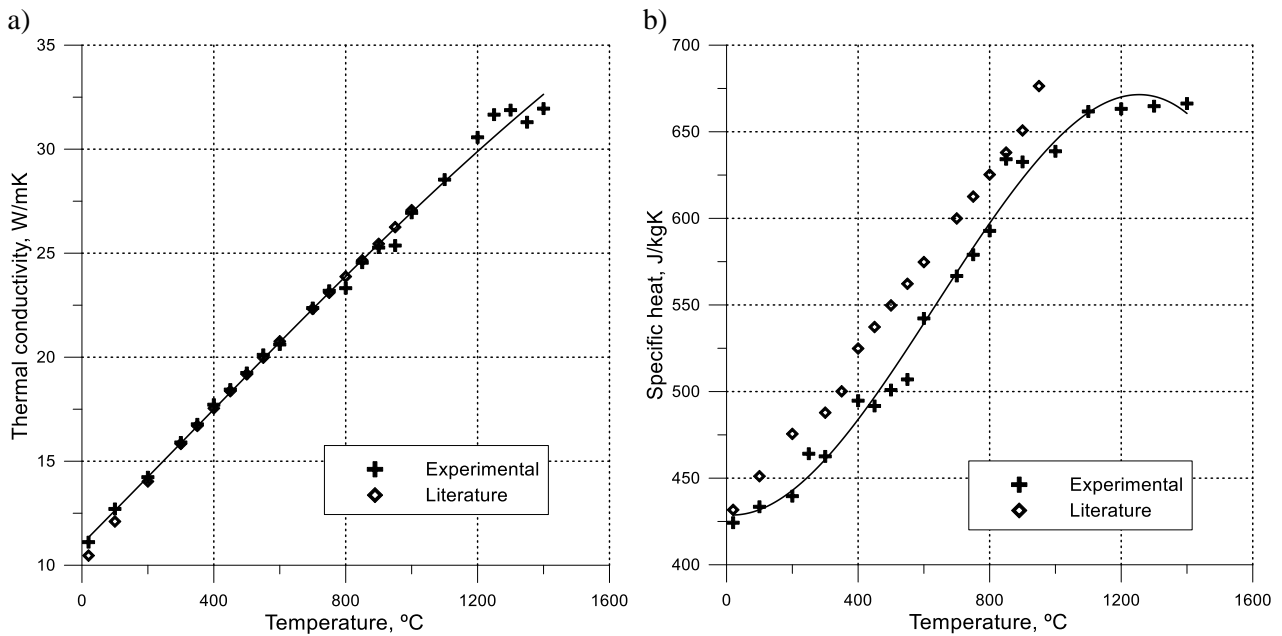


Fig. 5. Thermal conductivity (a) and specific heat (b) of Inconel 718 alloy versus temperature created for experimental and literature data [19]

### 3. EXPERIMENTAL RESULTS

Experimental and simulation studies of flat milling operations using a three tooth milling cutter shown in Fig. 2 were performed to expose the thermal image of the cutting zone. For simplicity, the fly milling with only one cutting tooth being in the contact with the workpiece was carried out. In this case, the distribution of cutting temperature is relatively easy to image.

As a result, it is possible to generate simple waveform recordings of the cutting temperature as a function of the rotation angle  $\phi$  of the milling cutter head. Their graphical visualizations for variable milling parameters are shown in Fig. 6.

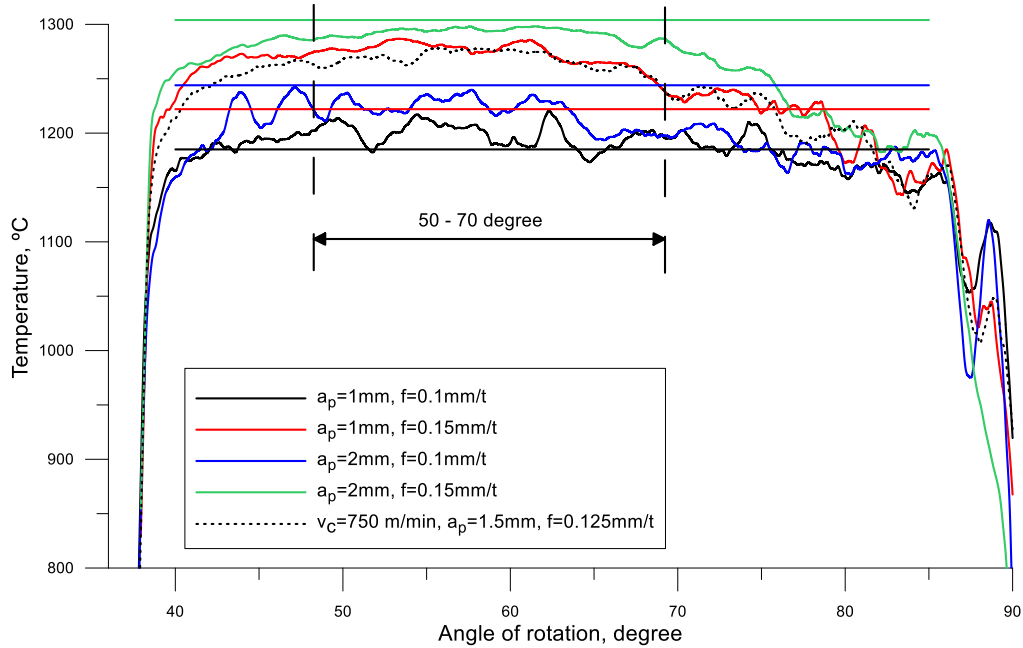


Fig. 6. Comparison of simulated cutting temperatures with minimum values of measured temperature (lines parallel to the X axis). Machining parameters:  $v_c=800$  and  $750$  m/min (only dotted line),  $a_p=1$  and  $2$  mm,  $f=0.1$  and  $0.15$  mm/tooth

It can be seen in Fig. 6 that for the selected set of machining parameters the average values of cutting temperature change in the range between  $1180^{\circ}\text{C}$  –  $1380^{\circ}\text{C}$ . The measured values of cutting temperature are specified in Table 3. It should also be noted in Fig. 6 that the instantaneous values of the cutting temperature were estimated by FEM modeling as function of the head rotation angle  $\psi$ . The region with maximum temperatures corresponds to the  $\psi$  angle between  $50^{\circ}$  and  $70^{\circ}$ . As a result, the average values of cutting temperature were determined for this machining period. The experimental results of mean, maximum and minimum cutting temperature for different cutting conditions are specified in Table 3.

Table 3. Experimental results of mean, maximum and minimum cutting temperature for different cutting conditions

| Cutting conditions |             |                 | Temperature, $^{\circ}\text{C}$ |                        |         |         |
|--------------------|-------------|-----------------|---------------------------------|------------------------|---------|---------|
| $v_c$<br>m/min     | $a_p$<br>mm | $f$<br>mm/tooth | Mean                            | Standard<br>deviations | Minimum | Maximum |
| 800                | 1.0         | 0.10            | 1236                            | 30                     | 1184    | 1279    |
| 800                | 1.0         | 0.15            | 1268                            | 28                     | 1222    | 1323    |
| 800                | 2.0         | 0.10            | 1286                            | 29                     | 1244    | 1341    |
| 800                | 2.0         | 0.15            | 1374                            | 19                     | 1304    | 1398    |
| 750                | 1.5         | 0.125           | 1293                            | 26                     | 1241    | 1340    |

In this case, the predicted values were validated using the average temperature values recorded by a high resolution IR camera. A representative temperature spectrum recorded with the average values determined are shown in Fig. 7.

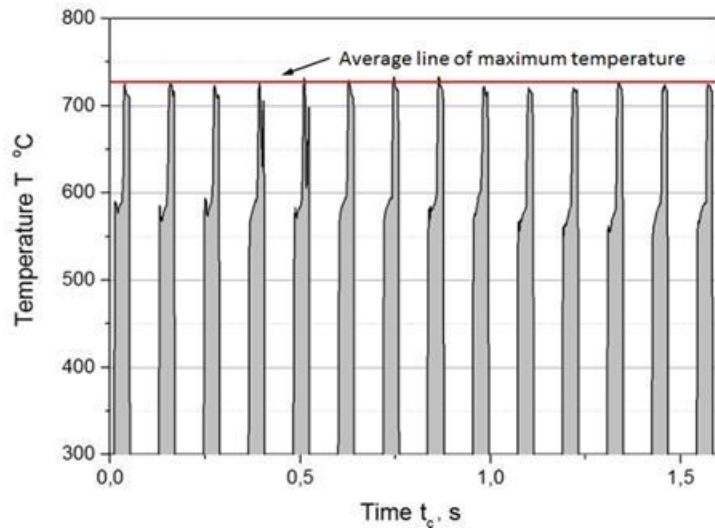


Fig. 7. Recorded temperature signal (by HD infrared camera) measured in the cutting zone with calculated average values of maximum temperature for 14 contacts areas of the cutting edge with the workpiece

It was observed that temperature changes recorded during cutter rotation are strongly related to the feed rate in such a way that higher temperatures occur for higher feed rate, independently of the depth of cut. These relationships are presented in Fig. 8. Moreover, the temperature signals generated at higher feed of 0.15 mm/tooth are more stable which coincides with the force signals.

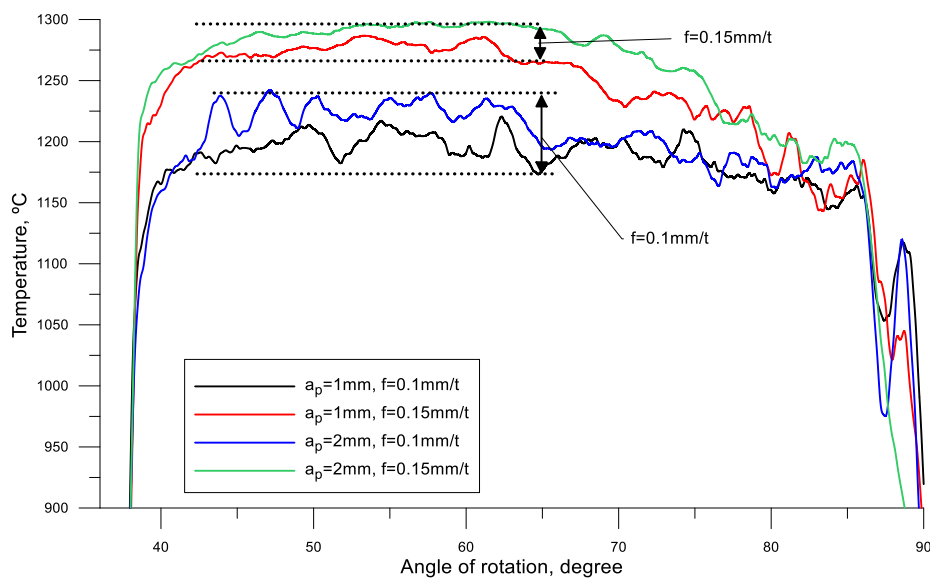


Fig. 8. Influence of feed rate on the changes of cutting temperature (grouping). Machining parameters:  $v_c=800$  m/min,  $a_p=1; 2$  mm,  $f=0.1; 0.15$  mm/tooth

Fig. 9 presents the comparison of measured and predicted values of the cutting temperature when varying the depth of cut and feed rate. The comparative algorithm was based on the Box-Whisker type graph where it was possible to assess the change of temperature values on the lower and upper quartile (bottom and top of the box respectively). It was also possible to assess the maximum fluctuation of the temperature value.

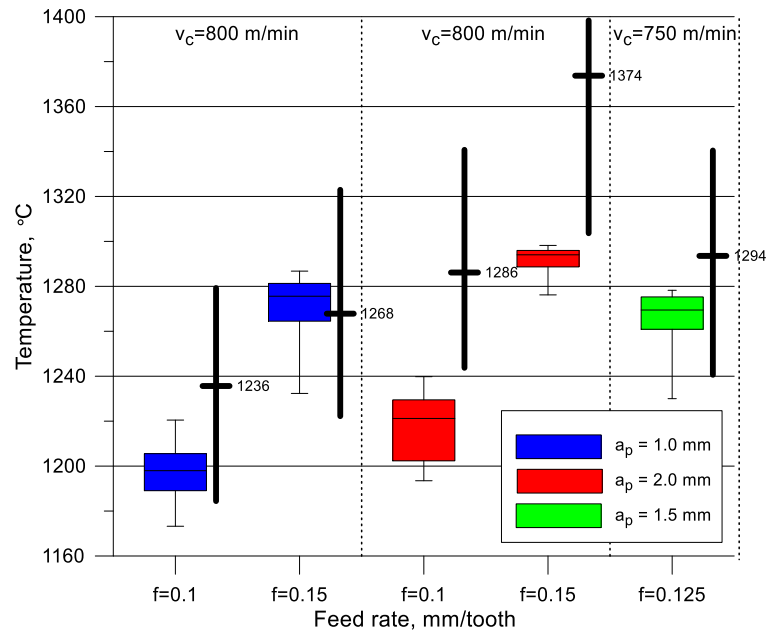


Fig. 9. Comparison of mean cutting temperature for experimental (black lines with mean and max-min range) and simulation results. Simulation results are presented in the form of the median and quartiles with the maximum values (Box-Whisker Plot)

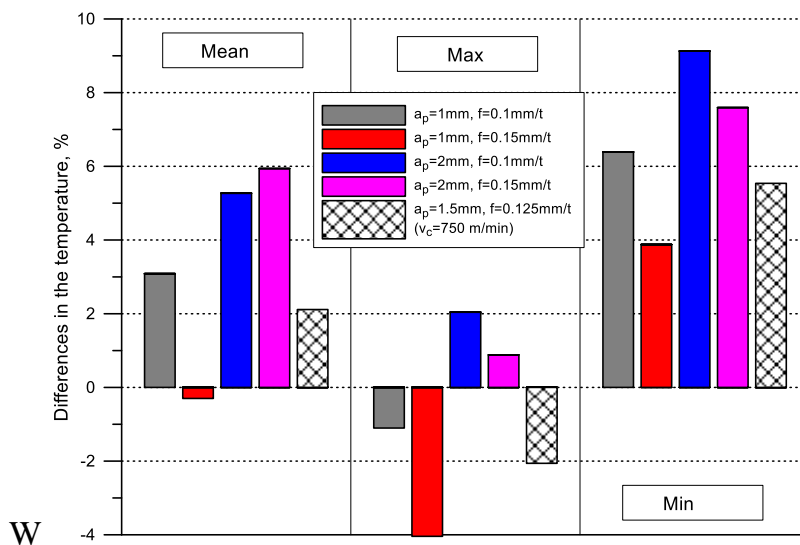


Fig. 10. Percentage differences in temperature in comparison to mean, maximum and minimum experimental data

It was observed that for the lower depth of cut  $a_p=1$  mm FEM simulations results agree satisfactorily for both feeds with measured result. Also a good agreement was achieved for a special milling test keeping  $v_c=750$  m/min,  $a_p=1.5$  mm and  $f=0.125$  mm/tooth. On the other hand, for a higher depth of cut of  $a_p=2$  mm experimental results overestimate the measured data. However, the changes of temperature resulting from increase of depth of cut are rather small.

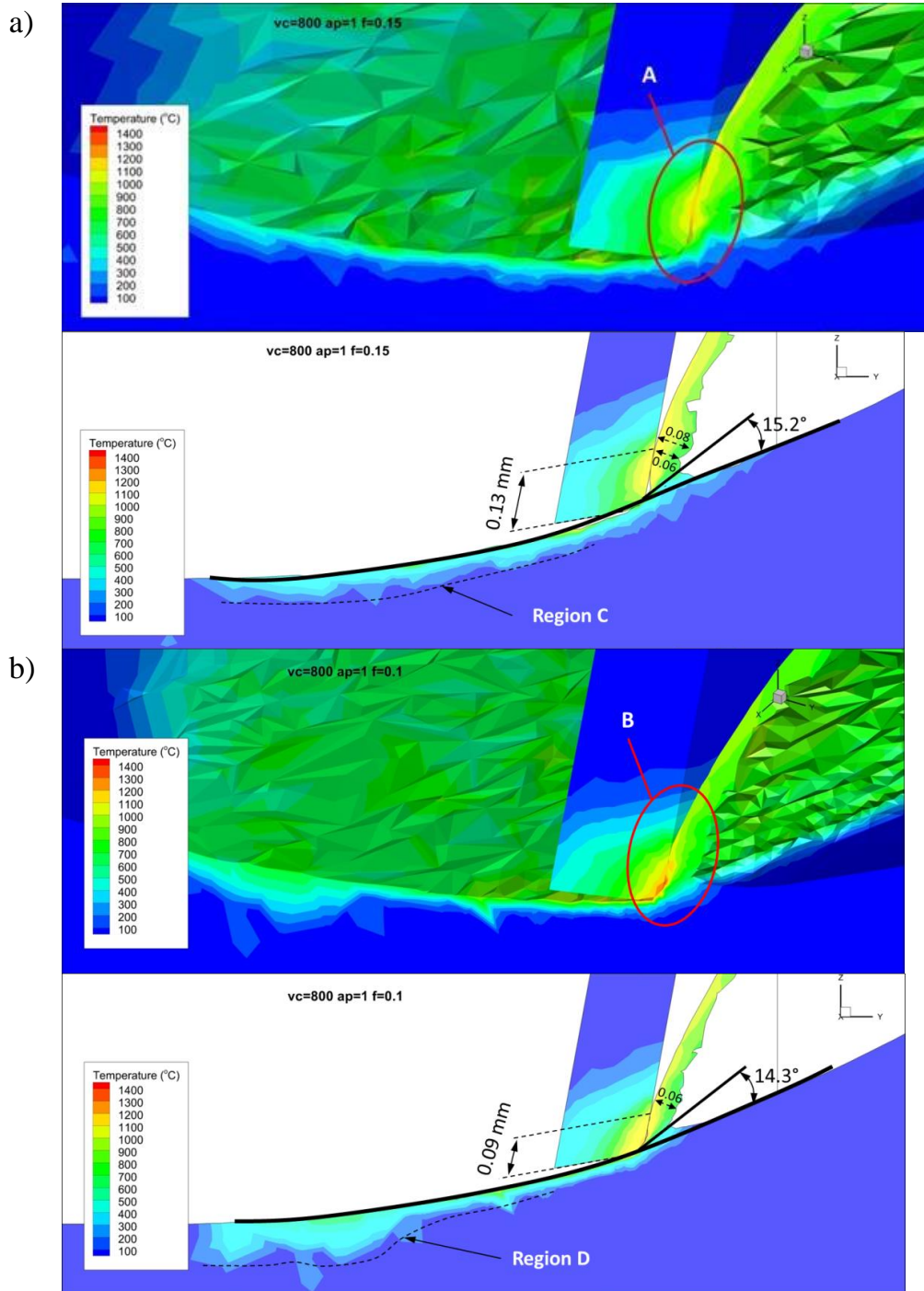


Fig. 11. Temperature distribution in the cutting zone for different feed rates and constant depth of cut obtained by using 3D and 2D slice technique. Machining parameters:  $v_c=800$  m/min,  $a_p=1$  mm, (a)  $f=0.15$  and (b)  $0.1$  mm/tooth

It should be noticed that in general the overall agreement between experimental and simulated data is good. Fig. 10 presents the percentage analysis of these differences.

It was performed with respect to the mean, maximum and minimum experimental values. In general, the differences between mean values do not exceed 6%. For the maximum values they range between -4% and 2% and for the minimum values they increase to 9% (the absolute error for the temperature of 1200°C is about +/- 50°C).

The temperature distributions in the cutting zone for the selected feed rates and depths of cut were visualized using a slice technique. The corresponding results obtained by using 3D and 2D slice technique for constant depth of cut of  $a_p = 1$  mm are presented in Fig. 11.

It was observed that the temperature distribution in the cutting zone depends on the feed rate. For the lower feed of 0.1 mm/tooth the high temperature zone is localized in the vicinity of the cutting edge, i.e. in zone B in Fig. 11. On the other hand, for the higher feed of 0.15 mm/tooth, for which the average temperature is higher, the high temperature zone is displaced from the cutting edge, i.e. zone "A" in Fig. 11. Similar effect was observed for the depth of cut of 2 mm. It can be noted that the specific heat of Inconel 718 at the temperature near 1200°C is relatively high and equal to 660 J/kg K and, as shown in Fig. 5b, it remains practically constant when temperature increases up to 1400°C. Because the feed determines the shear velocity, a higher feed causes that the heat is transferred faster from the contact zone and the higher temperature region is displaced from the cutting edge. For a lower feed the temperature field penetrates towards the workpiece to a greater extent, i.e. in Fig. 11 region D is more extended than C.

It was also observed in Fig. 11a and 11b that the feed influences the shear angle. When the feed rate decreases the shear angle decreases for both of depth of cut, as shown in Fig. 11. The shear velocity for  $a_p = 1$  mm, calculated using the shear angle value determined from FEM simulation, is in the range of 15.2 m/s for a lower feed rate and about 15.3 m/s for a higher feed. The increase of the depth of cut to 2 mm causes that the shear velocity decreases. Regardless of the feed rate used the differences are constant of about 0.6 m/s.

The feed also influences the tool-chip contact length. For  $a_p = 1$  i 2 mm and  $f = 0.1$  mm/t the tool-chip contact length  $l_c$  is equal to 0.09 (Fig. 11b) and 0.17 mm respectively. For the higher feed rate the  $l_c$  ranges from 0.13 to 0.22 mm for a lower and higher depth of cut.

When the tool-chip contact length increases, the heat transfer from the cutting zone becomes more intensive. As a result, for the feed of 0.15 mm/tooth, despite the higher average temperature, the temperature region with extremely high temperature does not appear.

#### 4. CONCLUSION

Constitutive model of workpiece material has a significant impact on the results of FEM simulation, especially in the area of mechanical and thermal influences [20]. Based on the experimental results and FEM predictions of the temperature distribution in the cutting area the conclusions are as follows:

- The J-C model results in a good compatibility of experiment and FEM simulation data in relation to the mean cutting temperature. In this case the differences between relevant temperatures are not higher than 9%.
- It was documented that the J-C model causes that the predicted results are more sensitive to changes of the feed rate. The temperature spectra are less stable for a lower feed rate.
- A good thermal comparison was obtained for FEM simulation and lower depth of cut ( $a_p=1$  mm). In this case the differences between predicted values of the average cutting temperature and experimental data, obtained for mean, maximum and minimum data range are not higher than 6%.
- It was observed that the temperature distribution maps in the cutting area are influenced by the feed rate. This effect was documented on the FEM simulations by analysing the areas of maximum temperature and the change of tool-chip contact length.

It is finally concluded, based on experiences resulting from this study, that the practical implementation of the most accurate constitutive material model and its thermophysical properties such as the thermal conductivity and the specific heat is very important. Additionally, it is extremely difficult and needs a number of advanced experiments for its validation.

#### ACKNOWLEDGMENTS

*Project co-financed by the European Regional Development Fund under the Operational Programme Innovative Economy and the National Centre for Research and Development Poland ( NCBR ) – Grant No. INNOLOT/I/7/ NCBR/2013 (2013-2018) - TED*

#### REFERENCES

- [1] UHLMANN E., Von Der SCHULENBURG M.G., ZETTIER R., 2007, *Finite element modeling and cutting simulation of inconel 718*, CIRP Ann. - Manuf. Technol., 56/1, 61–64.
- [2] ARRAZOLA P.J., ÖZEL T., UMBRELLO D., DAVIES M., JAWAHIR I.S., 2013, *Recent advances in modelling of metal machining processes*, CIRP Ann. - Manuf. Technol., 62/2, 695–718.
- [3] NIESŁONY P., GRZESIK W., HABRAT W., 2015, *Experimental and simulation investigations of face milling process of Ti-6Al-4V titanium alloy*, Adv. Manuf. Sci. Technol., 39, 39–52.
- [4] BUCHKREMER S., WU B., LUNG D., MÜNSTERMANN S., KLOCKE F., BLECK W., 2014, *FE-simulation of machining processes with a new material model*, J. Mater. Process. Technol., 214/3, 599–611.
- [5] NIESŁONY P., GRZESIK W., CHUDY R., LASKOWSKI P., HABRAT W., 2014, *3D FEM Simulation of Titanium Machining*, Int. Conference on Adv. Manufacturing Engineering and Technologies., 31–40.
- [6] YOO J.T., YOON J.H., LEE H.S., YOUN S.K., 2012, *Material characterization of Inconel 718 from free bulging test at high temperature*, J. Mech. Sci. Technol., 26/7, 2101–2105.
- [7] JAFARIAN F., IMAZ CIARAN M., UMBRELLO D., ARRAZOLA P.J., FILICE L., AMIRABADI H., 2014, *Finite element simulation of machining Inconel 718 alloy including microstructure changes*, Int. J. Mech. Sci., 88, 110–121.
- [8] GRZESIK W., NIESŁONY P., 2008, *FEM-based thermal modelling of the cutting process using power law-temperature dependent concept*, Arch. Mater. Sci. Eng., 29/2, 105–108.

- 
- [9] KLOCKE F., LUNG D., BUCHKREMER S., 2013, *Inverse identification of the constitutive equation of inconel 718 and AISI 1045 from FE machining simulations*, Procedia CIRP, 8, 212–217.
- [10] CHEN Y., BUNGET C., MEARS L., KURFESS T.R., 2013, *An Improved Empirical Constitutive Model for  $\gamma$  - Strengthened Nickel-Based Superalloys*, Proceedings of NAMRI/SME, 41.
- [11] NIESŁONY P., GRZESIK W., LASKOWSKI P., HABRAT W., 2013, *FEM-Based modelling of the influence of thermophysical properties of work and cutting tool materials on the process performance*, Procedia CIRP, 8, 3–8.
- [12] NIESŁONY P., GRZESIK W., LASKOWSKI P., SIENAWSKI J., 2014, *Numerical and Experimental Analysis of Residual Stresses Generated in the Machining of Ti6Al4V Titanium Alloy*, Procedia CIRP, 13, 78–83.
- [13] ZEMZEMI F., RECH J., BEN SALEM W., DOGUI A., KAPSA P., 2014, *Identification of friction and heat partition model at the tool-chip-workpiece interfaces in dry cutting of an inconel 718 alloy with cbn and coated carbide tools*, Adv. Manuf. Sci. Technol., 38/1, 5-22.
- [14] DEL PRETE A., FILICE L., UMBRELLO D., 2013, *Numerical simulation of machining nickel-based alloys*, Procedia CIRP, 8, 540–545.
- [15] PAWADE R.S., JOSHI S.S., 2011, *Mechanism of Chip Formation in High-Speed Turning of Inconel 718*, Mach. Sci. Technol., 15/1, 132–152.
- [16] CANTERO J.L., DÍAZ-ÁLVAREZ J., MIGUÉLEZ M.H., MARÍN N.C., 2013, *Analysis of tool wear patterns in finishing turning of Inconel 718*, Wear, 297/1–2, 885–894.
- [17] PUJANA J., ARRAZOLA P.J., SAOUBI R.M., CHANDRASEKARAN H., 2007, *Analysis of the inverse identification of constitutive equations applied in orthogonal cutting process*, Int. J. Mach. Tools Manuf., 47/14, 2153–2161.
- [18] NIESŁONY P., GRZESIK W., CHUDY R., HABRAT W., 2014, *Meshing strategies in FEM simulation of the machining process*, Arch. Civ. Mech. Eng., 1–9.
- [19] Material Properties Database, MPDB, JAHM Software, Inc., 2015.
- [20] NIESŁONY P., GRZESIK W., 2013, *Sensitivity Analysis of the Constitutive Models in Fem-Based Simulation of the Cutting Process*, J. Mach. Eng., 13/1, 106–116.